Int. J. Heat Mass Transfer. Vol. 20, pp. 1417–1425. Pergamon Press 1977. Printed in Great Britain

HEAT TRANSFER FROM ROTATING SHORT RADIAL BLADES

A. K. MOHANTY, T. S. RAGHAVACHAR and R. S. NANDA
Indian Institute of Technology, Kharagpur, India

(*Received* 9 *September* 1975 *and in revised form* 19 *January* 1977)

Abstract—Fluid flow and heat transfer from a rotating short radial blade is analysed, using rotating coordinate system, by Von Karman–Pohlhausen integral method, when the relative fluid motion is laminar. The transport rates for the blade are compared with those for a flat plate and for a rotating disk. Results of heat-transfer experiments, using blades of different included angles, are reported for both laminar and turbulent flow regimes, and are compared with theoretical predictions, as well as with other available data in the literature.

NOMENCLATURE

b_1, coefficient;
C, specific heat;
C_f, local skin friction coefficient;
C_f^*, $= C_f Re^{+1/2}$, characteristic skin friction coefficient;
$F(\eta, \theta)$, $= \dfrac{u}{\Omega r}$, velocity function in θ direction;
F', derivative of F w.r.t. η;
$G(\eta, \theta)$, $= \dfrac{v}{\Omega r}$, velocity function in r direction;
G', derivative of G w.r.t. η;
$H(\eta, \theta)$, $= \dfrac{w}{(\Omega\nu)^{1/2}}$, velocity function in z direction;
h, local heat-transfer coefficient;
K, thermal conductivity;
$M(\eta, \theta)$, $= \dfrac{T - T_z}{T_w - T_\infty}$, dimensionless temperature;
Nu, $= \dfrac{hr}{K}$, local Nusselt number based on radius;
Nu_θ, $= \dfrac{hr\theta}{K}$, local Nusselt number based on arc length;
Nu^*, $= \dfrac{h}{K(\Omega/\nu)^{1/2}}$, characteristic Nusselt number, $= Nu(Re)^{-1/2}$;
Pr, Prandtl number;
r, θ, z, cylindrical coordinates;
q, local heat flux per unit area;
T, temperature;
T_w, wall temperature;
T_∞, temperature of the ambient;
u, velocity component in the circumferential, θ direction;
v, velocity component in the radial, r direction;
w, velocity component in the z direction, normal to the plane of the plate;
Re, $= \dfrac{\Omega r^2}{\nu}$, local Reynolds number based on radius;
Re_θ, $= \dfrac{\Omega r^2 \theta}{\nu}$, local Reynolds number based on arc length.

Greek symbols

α, thermal diffusivity;
η, $= z(\Omega/\nu)^{1/2}$, dimensionless coordinate;
$\delta(\theta)$, hydrodynamic boundary-layer thickness;
$\delta^*(\theta)$, $= \delta(\Omega/\nu)^{1/2}$, dimensionless hydrodynamic boundary-layer thickness;
$\Delta(\theta)$, thermal boundary-layer thickness;
$\Delta^*(\theta)$, $= \Delta(\Omega/\nu)^{1/2}$, dimensionless thermal boundary-layer thickness;
$\xi(\theta)$, $= \dfrac{\Delta(Pr, \theta)}{\delta(\theta)}$, ratio of thermal to hydrodynamic boundary-layer thickness;
$\beta(\theta)$, $= \xi^3$;
ν, kinematic viscosity;
Ω, angular velocity of the rotating blade;
ρ, density;
τ_0, $= (\tau_{0r}^2 + \tau_{0\theta}^2)^{1/2}$, resultant local wall shear stress;
ε, $= \dfrac{G'(0)}{F'(0)}$, ratio of radial wall shear stress to circumferential wall shear stress.

1. INTRODUCTION

HEAT transfer from rotating surfaces is of considerable importance in engineering applications, and numerous studies involving transport phenomena from both symmetrical and unsymmetrical surfaces under rotation, where the centrifugal and Coriolis forces often significantly enhance the transport rates, have been reported in the literature over a period that extends as much as half a century. Heat transfer from turbine

disks, electrical machines, compressible fluid flow and heat transfer in high speed gas lubricated bearings are a few of the major examples of such application.

The hydrodynamics of fluid flow around a rotating body is three dimensional, and a classical example of an exact solution of the three dimensional Navier–Stokes equation exists for the case of a rotating disk [1]. The analytical and experimental studies of hydrodynamics and convective heat transfer from symmetric bodies under rotation have been summarised by Dorfman [2] and Kreith [3].

Flows over unsymmetrical bodies such as turbine blades are however, not amenable to closed form solution, because of the absence of angular symmetry. Analysis for long blades are made under the assumption of negligible cross flow [4, 5]. When the blades are short this assumption is untenable. Eisele *et al.* [6] presented an analysis for fluid flow relative to a rotating short rectangular blade under the restrictive assumption of radial shear stress being much smaller than its circumferential counterpart. The heat-transfer rate was estimated by applying Reynolds analogy.

Aside from the importance of the turbine blades, short blades can be gainfully used in rotating heat exchangers for enhanced transport rate due to centrifugal and Coriolis forces, and for simultaneous handling of the ambient fluid with lesser pressure drop, if the blades would be set at appropriate angles of incidence. However, published information on convective heat transfer, by analysis or from experiments with short rotating blades is too limited, practically non-existant for a radial blade, to undertake a satisfactory design of the type of heat exchanger envisaged. The present study is an attempt to make some progress in that direction.

In this paper, analysis of laminar fluid flow and heat transfer relative to a rotating short radial blade are considered. The restriction of negligible cross flow assumption is eliminated. Additionally, heat-transfer experiments were carried out using radial blades. The experimental results reasonably well corroborate the analytical predictions in the laminar regime, and provide information for heat transfer under turbulent flow conditions.

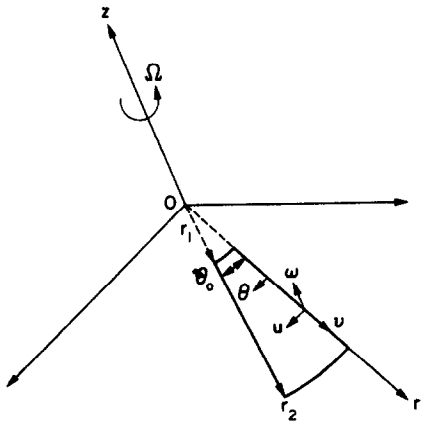

FIG. 1. Coordinate system, rotating with the blade.

2. ANALYSIS

2.1. *Velocity field*

Consider the rotation of a finite blade, rotating with uniform angular velocity Ω, in an unconfined mass of fluid extending to infinity. The blade is maintained at temperature T_w, while the temperature of the fluid far removed from the blade is assumed to be T_∞. The coordinate system, and the components of velocity in different direction are shown in Fig. 1.

Introducing dimensionless variables

$$\eta = Z(\Omega/\nu)^{1/2}, \quad F(\eta,\theta) = \frac{u}{\Omega r}, \quad G(\eta,\theta) = \frac{v}{\Omega r},$$

and $H(\eta,\theta) = w/(\Omega\nu)^{1/2}$, where ν is the kinematic viscosity, the boundary-layer form of the equations of continuity and momentum [6, 9] are written as

$$\frac{\partial F}{\partial\theta} + 2G + \frac{\partial H}{\partial\eta} = 0 \tag{1a}$$

$$F\frac{\partial F}{\partial\theta} + 2FG + H\frac{\partial F}{\partial\eta} - 2G = \frac{\partial^2 F}{\partial\eta^2} \tag{1b}$$

and

$$F\frac{\partial G}{\partial\theta} + G^2 + H\frac{\partial G}{\partial\eta} + 2F - F^2 - 1 = \frac{\partial^2 G}{\partial\eta^2} \tag{1c}$$

together with the boundary conditions

$$\eta = 0, \quad F = G = H = 0 \tag{2}$$
$$\eta \to \infty, \quad F = 1, \quad G = 0.$$

These equations are solved using the Karman–Pohlhausen method wherein the boundary conditions at infinity are replaced by the conditions at the edge of the boundary layer of thickness $\delta(\theta)$, or in dimensionless form, at $\delta^*(\theta) = \delta(\theta)\,(\Omega/\nu)^{1/2}$.

Equations (1b) and (1c), with the help of equation (1a) are recast into a set of two integro-differential equations by integrating between the limits $\eta = 0$ and $\eta = \delta^*$, as

$$\frac{\partial}{\partial\theta}\int_0^{\delta^*}(F^2 - F)\,d\eta + 4\int_0^{\delta^*} FG\,d\eta - 4\int_0^{\delta^*} G\,d\eta = -\frac{\partial F}{\partial\eta}\bigg)_{\eta=0} \tag{3}$$

and

$$\frac{\partial}{\partial\theta}\int_0^{\delta^*} FG\,d\eta + 3\int_0^{\delta^*} G^2\,d\eta + 2\int_0^{\delta^*} F\,d\eta - \int_0^{\delta^*} F^2\,d\eta = -\frac{\partial G}{\partial\eta}\bigg)_{\eta=0}. \tag{4}$$

The following polynomial expressions for F and G are assumed:

$$F(\eta,\theta) = \frac{3}{2}\left(\frac{\eta}{\delta^*}\right) - \frac{1}{2}\left(\frac{\eta}{\delta^*}\right)^3 \tag{5}$$

$$G(\eta,\theta) = b_1(\theta)\left|\left(\frac{\eta}{\delta^*}\right) - 3\left(\frac{\eta}{\delta^*}\right)^3 + 2\left(\frac{\eta}{\delta^*}\right)^4\right| - \frac{\delta^{*2}}{2}\left|\left(\frac{\eta}{\delta^*}\right)^2 - 2\left(\frac{\eta}{\delta^*}\right)^3 + \left(\frac{\eta}{\delta^*}\right)^4\right|. \tag{6}$$

These expressions have been chosen to satisfy the boundary conditions in (2) and the additional conditions:

$$\text{at } \eta = \delta^*, \quad \frac{\partial F}{\partial \eta} = \frac{\partial G}{\partial \eta} = 0$$

as freestream criteria, and

$$\text{at } \eta = 0, \quad \frac{\partial^2 F}{\partial \eta^2} = 0, \quad \frac{\partial^2 G}{\partial \eta^2} = -1. \tag{7}$$

The last set of boundary conditions in (7) are obtained by evaluating the momentum equations (1b) and (1c) at $\eta = 0$.

Substitution of expressions for F and G into equations (3) and (4) result in

$$\frac{d\delta^*}{d\theta} = -\frac{68}{39} b_1 \delta^{*2} + \frac{19}{117}\delta^{*3} + \frac{140}{13}\frac{1}{\delta^*} \tag{8}$$

and

$$\frac{db_1}{d\theta} = \frac{712}{975} b_1^2 - \frac{1699}{2925} b_1 \delta^{*2} - \frac{1428}{65}\frac{b_1}{\delta^{*2}} + \frac{547}{11700}\delta^{*4} + \frac{2153}{325} \tag{9}$$

which are to be solved for δ^* and b_1. The boundary layer is assumed to grow from the leading edge of the blade requiring that $\delta^* = 0$ at $\theta = 0$. This condition further requires that $b_1 = 0$ at $\theta = 0$, so that equation (9) is also satisfied at the leading edge.

2.2. *Temperature field*

The thermal boundary-layer equation pertinent to the problem, in dimensionless form, neglecting viscous dissipation, is obtained as [9]

$$F\frac{\partial M}{\partial \theta} + H\frac{\partial M}{\partial \eta} = \frac{1}{Pr}\frac{\partial^2 M}{\partial \eta^2} \tag{10}$$

with the boundary conditions

$$\eta = 0, \quad M = 1$$

and

$$\eta \to \infty, \quad M = 0 \tag{11}$$

where

$$M(\eta, \theta) = \frac{T - T_\infty}{T_w - T_\infty}.$$

Methods similar to the determination of velocity profile are used for obtaining temperature distribution in the thermal boundary layer of thickness Δ, non-dimensionalised as $\Delta^* = \Delta(\Omega/\nu)^{1/2}$. A temperature profile of the form

$$M(\eta, \theta) = 1 - \frac{3}{2}\left(\frac{\eta}{\Delta^*}\right) + \frac{1}{2}\left(\frac{\eta}{\Delta^*}\right)^3 \tag{12}$$

that satisfies the essential boundary conditions given in (11) as modified to hold good at the edge of the boundary layer, and additional conditions

$$\text{at } \eta = \Delta^*, \quad \frac{\partial M}{\partial \eta} = 0 \tag{13}$$

and

$$\text{at } \eta = 0, \quad \frac{\partial^2 M}{\partial \eta^2} = 0 \tag{14}$$

obtained by applying the wall conditions to the energy equation, are selected.

The integrated forms of equation (10) are

$$\frac{\partial}{\partial \theta}\int_0^{\Delta^*} GM\, d\eta + \int_0^{\Delta^*} 2GM\, d\eta = -\frac{1}{Pr}(\partial M/\partial \eta)_{\eta=0} \tag{15}$$

when $\delta^* > \Delta^*$ and

$$\frac{\partial}{\partial \theta}\int_0^{\delta^*} GM\, d\eta + \int_0^{\delta^*} 2GM\, d\eta + \int_{\delta^*}^{\Delta^*} M\, d\eta = -\frac{1}{Pr}\left(\frac{\partial M}{\partial \eta}\right)_{\eta=0} \tag{16}$$

when $\delta^* < \Delta^*$.

Substitution of the expressions for F, G and M in equations (15) or (16), and use of the definitions $\xi = \Delta^*/\delta^*$, $\beta = \xi^3$, lead to

$$\frac{d\beta}{d\theta} = \frac{105}{(7-\beta^{2/3})}\frac{\beta}{\delta^{*2}}\left| \beta^{1/3}\left(\frac{5}{18}\delta^{*4}\right) - \beta^{2/3}\left(\frac{449}{1638}\delta^{*4} - \frac{200}{273}b_1\delta^{*2} - \frac{10}{13}\right) + \beta\left(\frac{1}{12}\delta^{*4} - \frac{1}{3}b_1\delta^{*2}\right) - \frac{4}{3}b_1\delta^{*2} + \frac{68}{39}b_1\delta^{*2} - \frac{19}{117}\delta^{*4} - \frac{140}{13}\right| + \frac{1}{Pr}\frac{105}{(7-\beta^{2\,3})\delta^{*2}} \tag{17}$$

when $\delta^* > \Delta^*$

$$\frac{d\beta}{d\theta} = \frac{840}{\delta^{*2}}\frac{\beta}{(42\beta^{2/3} - 9 - 105\beta^{4/3})} \times \left| \left(\frac{62}{65}b_1\delta^{*2} - \frac{49}{520}\delta^{*4} - \frac{105}{26}\right)\beta + \beta^{2/3}\left(-\frac{6}{13}b_1\delta^{*2} + \frac{77}{1560}\delta^{*4} + \frac{29}{13} - \frac{3}{2Pr}\right) + \beta^{4/3}\left(-\frac{17}{26}b_1\delta^{*2} + \frac{19}{312}\delta^{*4} + \frac{105}{26}\right) + \left(\frac{73}{1820}b_1\delta^{*2} - \frac{103}{21840}\delta^{*4} - \frac{3}{26}\right)\right| \tag{18}$$

when $\delta^* < \Delta^*$.

The initial values for β, for any value of Pr, is obtained by treating $d\beta/d\theta = 0$ at $\theta = 0$ in equations (17) and (18). This assumption is based on the observation that it leads to $\xi = 1$ at $\theta = 0$, for $Pr = 1$.

Equations (8), (9) and (17) or (18) are solved for different values of Pr in the range 0.1 to 100, by numerical computation using fourth order Runge–Kutta method.

2.3. *Results of the analysis*

The results of the foregoing anslyses, both for fluid flow and convective heat transfer relative to a rotating short radial blade, under laminar condition, can now be summarised. The only other available results for a short rectangular rotating blade are those of Eisele *et al.* [6]. Their analysis is however, limited to only fluid flow, made under the restrictive assumption of $\tau_{0r} \ll \tau_{0\theta}$, unlike in the present analysis where no such assumption is made *a priori*. Furthermore, in a rectangular blade, the blade included angle varies from the root to the tip, and as such Eisele's results are not directly comparable with those of the present analysis. Nevertheless, reference is made to Eisele's results wherever desirable, for completeness.

(i) *Boundary layers.* The development of the hydrodynamic and the thermal boundary layers from the leading edge of the blade is indicated in Fig. 2. The corresponding results for a flat plate [7] and for a rotating disk are also given for comparison. The results for the rotating disk are obtained as a special case by setting $d\delta^*/d\theta = 0$ and $db_1/d\theta = 0$, in equations (8) and (9).

For comparison with the blade, the characteristic dimension for a flat plate is chosen as $r\theta$, equal to the blade arc length, and for the disk the dimension is the radius r.

It can be seen that for blade angles up to 0.3 rad the dimensionless hydrodynamic boundary-layer thickness is almost identical with that on a flat plate. As the blade angle increases the boundary layer deviates from the flat plate value and tends asymptotically to the rotating disk value for $\theta > 2$ radians. A similar trend is exhibited by the thermal boundary layer, Δ^*, the asymptotic value being attained at lesser blade angles as the Prandtl number increases.

(ii) *Velocity and temperature functions.* The velocity and the temperature functions, F, G and M, across the boundary layer at selected blade angles are presented in Fig. 3, together with the calculated profiles for a rotating disk. It is noted that at small blade angles, the relative magnitude of the radial velocity function G is small and thus the flow could be treated as two-dimensional. At larger blade angles, the maximum value and the gradient of G become appreciable.

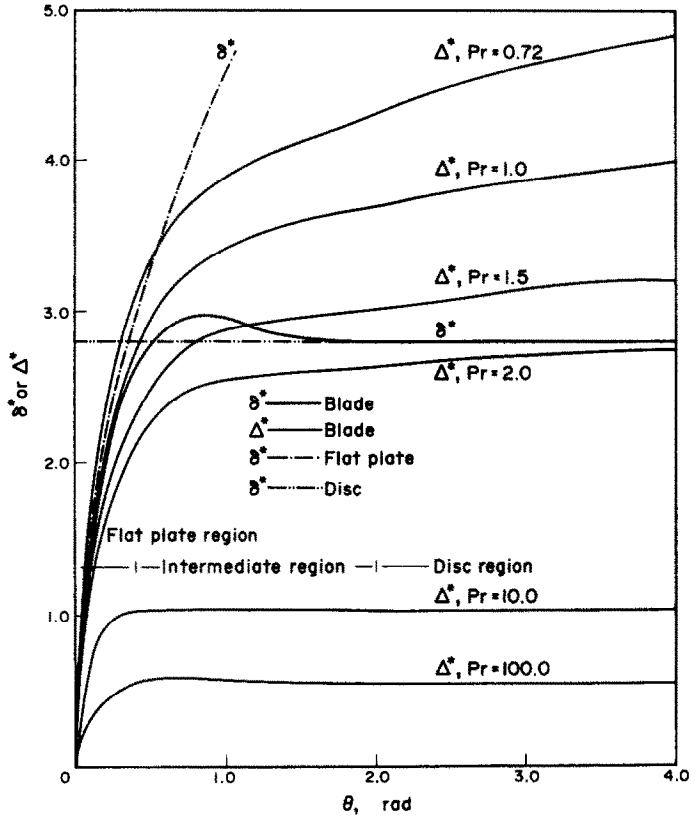

FIG. 2. Hydrodynamic and thermal boundary layers.

(iii) *Wall shear stress.* The wall shear stresses in the θ and r directions can be calculated as

$$\tau_{0\theta} = \mu\left(\frac{\partial u}{\partial z}\right)_{z=0} = \mu\Omega r(\Omega/\nu)^{1/2}F'(0)$$

and

$$\tau_{0r} = \mu\left(\frac{\partial v}{\partial z}\right)_{z=0} = \mu\Omega r(\Omega/\nu)^{1/2}G'(0).$$

Defining the resultant wall shear stress as

$$\tau_0 = (\tau_{0\theta}^2 + \tau_{0r}^2)^{1/2},$$

and the local skin friction coefficient as

$$C_f = \frac{\tau_0}{1/2\rho U_\infty^2},$$

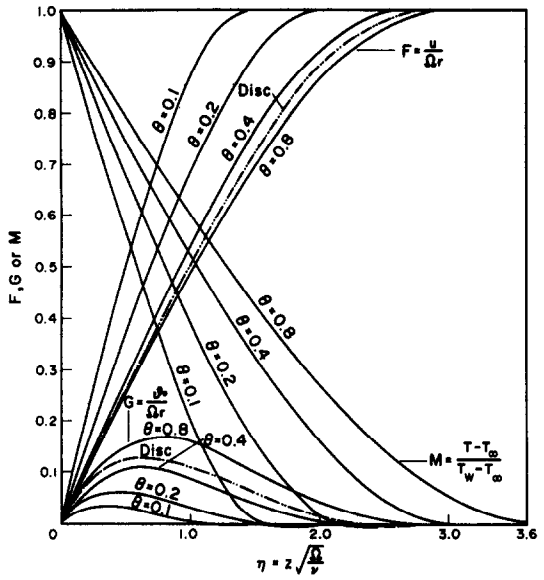

FIG. 3. Velocity and temperature functions.

where $U_\infty = \Omega r$, it is obtained that

$$C_f = \frac{2F'(0)(1+\varepsilon^2)^{1/2}}{r(\Omega/\nu)^{1/2}}, \tag{19}$$

where

$$\varepsilon = \frac{G'(0)}{F'(0)}.$$

Equation (19) leads to the definition of a characteristic skin friction coefficient as

$$C_f^* = C_f Re^{1/2} = 2F'(0)(1+\varepsilon^2)^{1/2} \tag{20}$$

where $Re = \Omega r^2/\nu$.

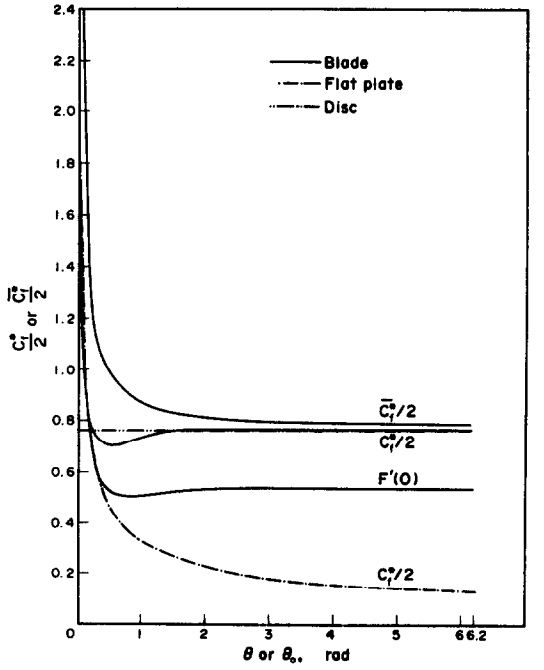

FIG. 4. Local and average skin friction coefficients.

The advantage of using a characteristic coefficient lies in its independence of blade geometry, especially of the radius. A similar definition, as will be seen later, is also applicable for the heat-transfer rate.

The average value of the skin friction is evaluated by numerical integration,

$$\bar{C}_f = \frac{1}{A}\int_{r_1}^{r_2}\int_0^{\theta_0} C_f r \, d\theta \, dr$$

and the corresponding characteristic value is $\bar{C}_f^* = \bar{C}_f(\Omega r_m^2/\nu)^{1/2}$, where $r_m = (r_1+r_2)/2$.

The local and the average variation of C_f^* are plotted in Fig. 4. For the sake of comparison, the corresponding results for a flat plate and for a rotating disk are also given. It is assumed for the flat plate that [7]

$$C_{f/2} = 0.323 Re_\theta^{-1/2}, \quad Re_\theta = \frac{\Omega r^2 \theta}{\nu},$$

the coefficient 0.323 being compatible for approximate analysis. The rotating disk results are estimated from equations (8) and (9) by applying angular symmetry, as

$$C_{f/2} = 0.763 Re^{-1/2}.$$

Hence

$$C_{f/2}^* = 0.323\theta^{-1/2} \tag{21}$$

for a flat plate of characteristic length $r\theta$, and

$$C_{f/2}^* = 0.763 \tag{22}$$

for a rotating disk.

The local C_f^* value for a blade at blade angles less than 0.3 rad, is almost identical with that of a flat plate; at large angles ($\theta > 1.5$ rad) the disk value is attained asymptotically. The average value of the skin friction coefficient, $\bar{C}_f^*$, for a blade is however, higher than the flat plate or the disk value, for the respective range of blade included angles. The increase in average value for a blade over a flat plate at small angles can be attributed to the three dimensional flow condition, and to the presence of a leading edge when compared with a disk.

(iv) *Heat transfer.* The local heat-transfer coefficient for an isothermal blade is,

$$h = \frac{-K(\partial T/\partial z)_{z=0}}{T_w - T_\infty}$$

$$= -K(\Omega/\nu)^{1/2}\left(\frac{\partial M}{\partial \eta}\right)_{\eta=0}.$$

This leads to the definition of a characteristic Nusselt number,

$$Nu^* = \frac{h}{K(\Omega/\nu)^{1/2}} = \frac{3}{2\Delta^*}. \tag{23}$$

Following the procedures already indicated for estimating C_f^* and $\bar{C}_f^*$, the characteristic Nusselt number for a glat plate and for a rotating disk are written respectively as,

$$Nu^* = Nu_\theta Re_\theta^{-1/2}\theta^{-1/2} = 0.323\theta^{-1/2}$$

for a flat plate [7] and

$$Nu^* = NuRe^{-1/2} = 0.396$$

for a disk [8].

For $Pr = 1$, the variation of Nu^* with blade angle and comparison with the flat plate and the disk values are indicated in Fig. 5. Similar conclusions as for C_f^* are noted.

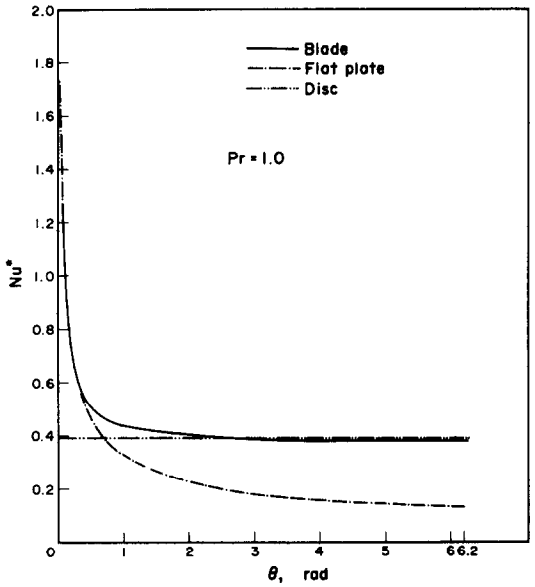

FIG. 5. Comparison of local heat-transfer coefficients.

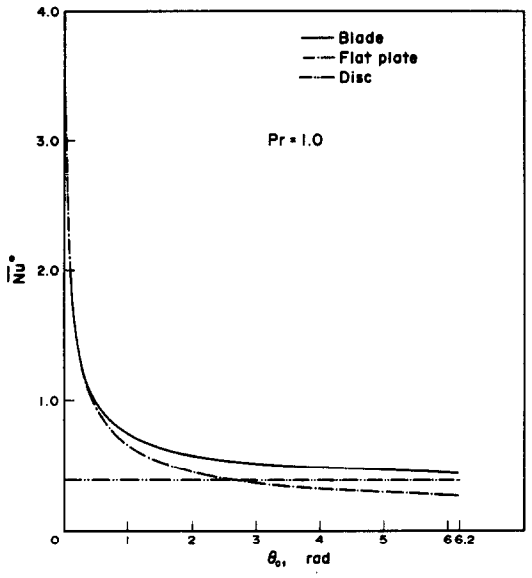

FIG. 6. Comparison of average heat-transfer coefficients.

The average heat transfer expressed through $\overline{Nu}^*$ is obtained by numerical integration and is given in Fig. 6 for different values of the blade included angle. The average values for a flat plate and for a disk are also given. For blade included angles θ_0, over 0.4 rad, the average heat transfer from the radial blade is higher than both the flat plate and the disk values. The improvement in the heat-transfer rate is greater than the increase in the skin friction coefficient (Fig. 4). This signifies that higher heat-transfer rates can be achieved by using rotating radial blades, with less than proportionate increase in skin friction loss.

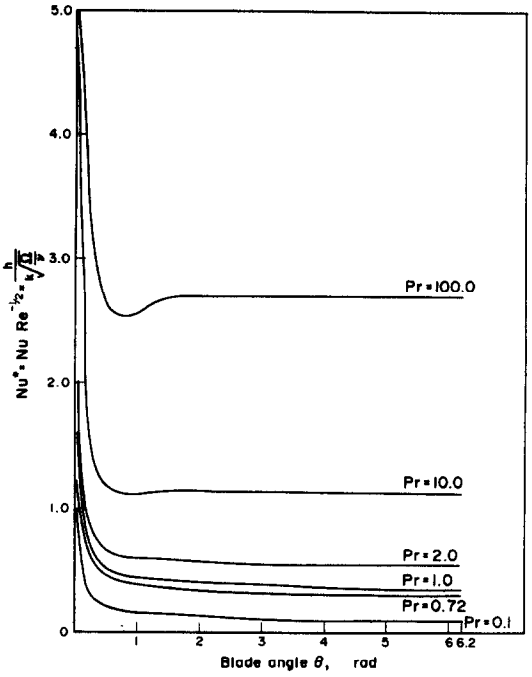

FIG. 7. Local heat-transfer coefficients.

The effect of Prandtl number on the rate of heat transfer from a rotating radial blade is indicated in Fig. 7.

3. EXPERIMENTS

Heat-transfer experiments were carried out using short radial blades of approximately 15 cm radial dimension. The blades were of included angles 10, 15, 30, 45, 60 and 90°, and were heated electrically by nichrome wire heating elements. Two separately controlled heating elements were used to obtain isothermal blade surface. The heater power supply and blade temperature measurements were carried out by means of slip rings, with arrangement for the control of individual spring tension, and with compensating thermocouples. A schematic diagram of the experimental set up is given in Fig. 8. Further details of the apparatus and method of calibrations that ensured elimination of errors due to frictional and differential heating at the thermocouple slip ring-brush junction, the error due to the presence of electric heater, as well as the details of theoretical analysis are available in [9].

Either two or four number of statically balanced blades of each of the above included angles were used. Only one blade was heated and the ambient temperature was measured by a thermocouple located in one of the other (dummy) blades. The rotational speed was varied from 50 to 1000 rev/min.

3.1. *Results of the experiments*

For brevity, only results of experiments with 10° and 15° (included angle) blades are shown in Fig. 9.

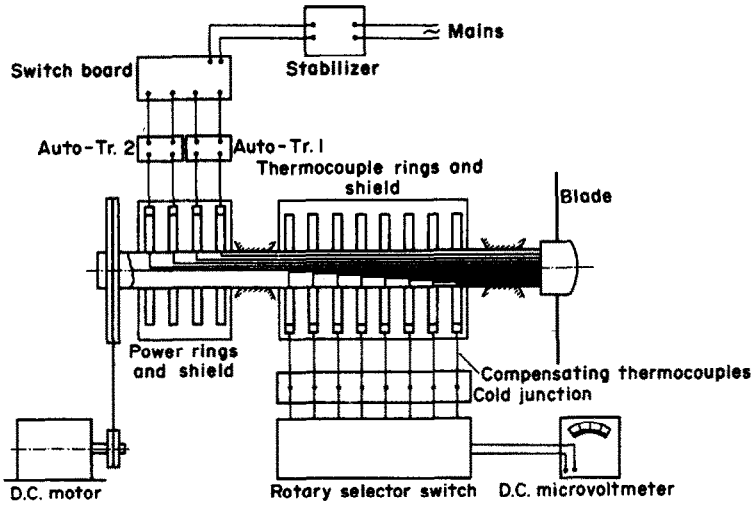

FIG. 8. Apparatus for thermal measurements.

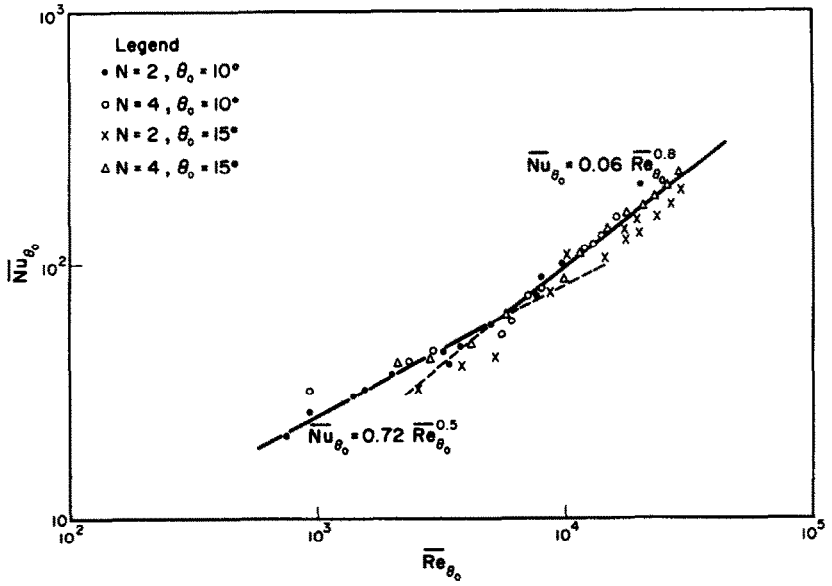

FIG. 9. Heat transfer at zero incidence angle.

However, correlation of experimental results of other categories of blades are also given. The choice of variables and coordinates for presenting the experimental results are guided by the finding of the theoretical analysis, which in brief is, that the blades of small included angle be comparable with a flat plate and those of the large included angle with a rotating disk.

For blades of included angles 10° and 15° ($\theta_0 < 0.4$ radians) the experimental results are correlated as

$$\overline{Nu_\theta} = 0.72\overline{Re_\theta^{0.5}}$$

for laminar, and as

$$\overline{Nu_\theta} = 0.06\overline{Re_\theta^{0.8}}$$

for turbulent regimes.

The laminar result is thus seen to be in good agreement with the result of a flat plate, and consequently with the theoretical predictions for blades of small included angles. For the turbulent regime, the blade result is about 50% higher than the flat plate result where the coefficient is usually 0.037, for $Pr = 1$ [7]. The transition to turbulent flow is observed to take place at $\overline{Re_\theta} = 5 \times 10^3$, which is about two orders of magnitude less than that for a flat plate [7].

Eisele *et al.* [6] reported for rectangular blades, for which the included angle varies from root to tip and hence are not very compatible for comparison with radial blades, a value of $\overline{Nu_\theta} = 0.036\overline{Re_\theta^{0.8}}$.

The average heat-transfer rate from blades of 45, 60 and 90° included angles could be correlated on a single plot of $\overline{Nu}$ vs $\overline{Re}$, confirming the theoretical postulation of disk type behaviour, as

$$\overline{Nu} = 0.95\overline{Re^{0.5}}$$

in the laminar regime and as

$$\overline{Nu} = 0.0415\overline{Re^{0.8}}$$

in the turbulent regime, with the transition taking place at an approximate value of $\overline{Re} = 3 \times 10^4$.

Noting the definitions that $\overline{Nu^*} = \overline{NuRe}^{-0.5}$, it is seen that the laminar result for the blades of large included angles are about 30% higher than the theoretically predicted value, when $Pr = 1$ (Fig. 6). Experimental results for heat transfer in the turbulent regime from a rotating disk are reported in the literature [10] as

$$\overline{Nu} = 0.0151\overline{Re}^{0.8} \text{ in air,}$$
$$Pr = 0.72.$$

The experimental results for the blades are thus observed to be more than two times the reported values for a disk [8].

Results of experiments with 30° blade (included angle) could not be correlated by expressions obtained either for blades of small (10 and 15°) or of large (45, 60 and 90°) included angles. The 30° blades, for which the transport rate was experimentally estimated to be higher than the blades of larger included angles, can be considered as a blade of the intermediate region, Fig. 2.

Limited experiments were also performed with 10 and 15° blades when the blades were set at an angle of incidence. An incidence angle of 25° was observed to be the threshold value for enhancing the heat-transfer rate. This can be partly attributed to the presence of axial flow when blades are set at incidence.

4. SUMMARY

The three dimensional laminar fluid flow and heat transfer relative to a rotating short radial blade at zero angle of incidence have been analysed by the application of the Von Karman–Pohlhausen integral technique. Simplifying assumption of either negligible cross flow, as is usually made with long blades [4, 3], or that the radial shear stress is much smaller than its circumferential counterpart, as was made with a short rectangular blade [6], has been dispensed with. The average transport rate from a rotating blade is higher than that from a flat plate due to three dimensional flow, and is high compared to a disk due to the presence of a leading edge.

Heat-transfer experiments have been performed with radial blades of included angle that can be said to cover the range of small, intermediate and large blade angles. The experiments corroborate the validity of the theoretical analysis in the laminar regime, especially for small blade angles. Heat-transfer rates at turbulent conditions have been obtained only experimentally. The blade values in the turbulent regime also are higher than those for the flat plate or the disk. Transition to turbulent regime appears to occur at relatively lower Reynolds number.

REFERENCES

1. H. Schlichting, *Boundary Layer Theory*. McGraw-Hill, New York (1968).
2. L. A. Dorfman, *Hydrodynamic Resistance and the Heat Loss of Rotating Solids*. Oliver and Boyd, Edinburgh (1963).
3. F. Kreith, Convective heat transfer in rotating systems, in *Advances in Heat Transfer*, Vol. 5, pp. 129–251. Academic Press, New York (1968).
4. L. E. Fogarty, The laminar boundary layer on a rotating blade, *J. Aeronaut. Sci.* **18**, 247–252 (1951).
5. H. S. Tan, On laminar boundary layer over a rotating blade, *J. Aeronaut. Sci.* **20**, 780–781 (1953).
6. E. H. Eisele, W. Leidenfrost and A. E. Muthunayagam, Studies of heat transfer from rotating heat exchangers, in *Progress in Heat and Mass Transfer*, Vol. 2, pp. 483–499. Pergamon Press, Oxford (1969).
7. E. R. G. Eckert and R. M. Drake, Jr., *Heat and Mass Transfer*. McGraw-Hill, New York (1959).
8. E. M. Sparrow and J. L. Gregg, Heat transfer from a rotating disk to a fluid of any Prandtl number, *J. Heat Transfer* **81**, 249–250 (1959).
9. T. S. Raghavachar, Heat transfer from rotating short radial blades, Ph.D. thesis, Indian Institute of Technology, Kharagpur, India (1976).
10. E. C. Cobb and O. A. Saunders, Heat transfer from a rotating disk, *Proc. R. Soc.* **A236**(1206), 342–351 (1956).

TRANSFERT THERMIQUE PAR DES AILETTES COURTES ET RADIALES EN ROTATION

Résumé—On analyse l'écoulement et le transfert thermique autour d'une ailette courte, radiale et en rotation, en utilisant un système de coordonnées tournant et la méthode intégrale de Von Karman–Pohlausen, dans le cas du mouvement relatif laminaire. Les flux de tranfert pour l'ailette sont comparés à ceux d'une plaque plane et d'un disque tournant. Des résultats d'expérience sur différents angles sont donnés à la fois pour les régimes laminaires et turbulents et sont comparés aux calculs et aux autres résultats tirés de la bibliographie.

DER WÄRMEÜBERGANG AN ROTIERENDEN, KURZEN RADIALSCHAUFELN

Zusammenfassung—Unter Zugrundelegung eines rotierenden Koordinatensystems werden Strömung und Wärmeübergang an einer rotierenden, kurzen Radialschaufel untersucht. Bei laminarer Relativströmung wird die Von-Karman–Pohlhausen-Integralmethode verwendet. Die Austauschraten für die Schaufel werden mit denen für ebene Platten und rotierende Scheiben verlichen. Für den Wärmeübergang an Schaufeln verschiedener Anstellwinkel werden Versuchsergebnisse bei laminarer und turbulenter Strömung angegeben; sie werden mit theoretisch errechneten Werten und mit Literaturangaben verlichen.

ПЕРЕНОС ТЕПЛА ОТ ВРАЩАЮЩИХСЯ РАДИАЛЬНЫХ ЛОПАСТЕЙ НЕБОЛЬШИХ РАЗМЕРОВ

Аннотация — С помощью интегрального метода Кармана–Польгаузена во вращающейся системе координат анализируются процессы обтекания и теплообмена радиальной лопасти небольшого размера, вращающейся в ламинарном потоке жидкости. Проводится сравнение скоростей переноса для лопасти, плоской пластины и вращающегося диска. Полученные результаты экспериментального исследования процесса теплообмена лопастей, расположенных под различными углами как в ламинарном, так и турбулентном потоке, сравниваются с результатами теоретических расчетов и данными других авторов.